Wear 318 (2014) 27–39

Contents lists available at ScienceDirect

Wear

journal homepage: www.elsevier.com/locate/wear

A friction model for loading and reloading effects in deep drawing processes ☆

D.K. Karupannasamy [a,b,*], J. Hol [a,c], M.B. de Rooij [b], T. Meinders [c], D.J. Schipper [b]

[a] Materials innovation institute (M2i), P.O. box 5008, 2600 GA Delft, The Netherlands
[b] University of Twente, Faculty of Engineering Technology, Laboratory for Surface Technology and Tribology, P.O. box 217, 7500 AE Enschede The Netherlands
[c] University of Twente, Faculty of Engineering Technology, Nonlinear solid mechanics, P.O. box 217, 7500 AE Enschede, The Netherlands

ARTICLE INFO

Article history:
Received 3 January 2014
Received in revised form
8 June 2014
Accepted 9 June 2014
Available online 18 June 2014

Keywords:
Friction model
Deep drawing process
Asperity flattening
Ploughing
Boundary lubrication

ABSTRACT

Deep drawing is one of the most widely-used forming processes to manufacture automotive body parts from sheet metal. In order to simulate deep drawing processes, a finite element (FE) method was used to predict formability. The accuracy of the FE simulation depends on the material models, numerical techniques, and contact algorithms. Despite the fact that the contact conditions between the tool and sheet material influences the coefficient of friction in forming processes, the coefficient of friction is often treated as a constant Coulomb friction coefficient in FE simulations. However, a friction model based on local contact conditions and surface topography is required to improve forming predictability. There is growing interest in developing contact models to predict the nature of friction conditions for use in FE calculations. In deep drawing processes, the sliding contact predominantly occurs in the blank holder region between the tool and sheet material. The contact pressure in the blank holder is non-uniform due to bending and material compression which vary depending on tool geometry. The sheet metal surface is subjected to repeated contact during sliding, which in turn affects the local friction conditions. The objective of this paper is to develop a sliding friction model for mixed modes of surface deformation. The deterministic approach used in the current model includes the roughness of both the sheet material and the tool. The sheet material is subject to an asperity flattening process. Further, the tool surface indents into the sheet material under normal loading. The geometry of the asperities is characterized by an elliptical paraboloid shape to better calculate the load-dependence of friction. The model has been compared with data from experiments using a rotational friction tester under multiple loading conditions.

1. Introduction

1.1. Contact conditions in deep drawing processes

Deep drawing process involves the forming of the sheet metal to the required shape using a die and punch. Complex contact conditions occur between the sheet metal and tool when sliding over the die rounding region due to the combined bending and tensile forces [1] as shown in Fig. 1. The contact pressure is not uniform in the blank holder and die rounding regions and the sheet metal surface is subjected to repeated contacts under varying loads. For example, when the sheet material slides over the die rounding region (marked as 1–3 in Fig. 1) the surface is locally loaded to a high contact pressure followed by lower contact pressures. At the micro-scale, the contact occurring between the surfaces is discrete. The surface topography is composed of micro irregularities, called as asperities. The formation of junctions at the micro-contacts due the application of load governs the friction as proposed by Tabor [2]. The junction theory has been further used to develop contact models to describe surface deformation process. Statistical methods have been developed by Greenwood and Williamson [3] and Pullen and Williamson [4] to describe the surface deformation process. For metal forming processes, the surface deformation is complex and the contact models have been extended to describe the bulk deformation process by Wilson and Sheu [5] and Sutcliffe [6] using a wedge shaped asperity for plane stress and strain conditions. Various experimental techniques have also been developed to measure the coefficient of friction by simulating the conditions occurring in deep drawing processes. The choice of experiment depends on how the deformation behaviour is controlled. For a simple deep drawing process (for example cup drawing test or U-shaped strip drawing test) as a test method, punch forces can be measured to quantify the effect of surface roughness and lubrication effects.

☆This paper was presented at the 2013 World Tribology Congress.

* Corresponding author at: Materials innovation institute (M2i), P.O. box 5008, 2600 GA, Delft, The Netherlands. Tel.: +31 534894325; fax: +31 534894784.
E-mail addresses: k.dineshkumar@yahoo.co.in, d.karupannasamy@m2i.nl (D.K. Karupannasamy).

http://dx.doi.org/10.1016/j.wear.2014.06.011
0043-1648/

Nomenclature

a	semi-major radius of elliptical paraboloid asperity [m]
b	semi-minor radius of elliptical paraboloid asperity [m]
f_d	boundary layer degradation factor [dimensionless]
f_{hk}	interfacial friction factor [dimensionless]
h	surface separation [m]
k	shear strength of deforming material [Pa]
m	elliptic integral parameter [dimensionless]
A	contact area of an asperity [m^2]
C_A	critical contact area at the onset of plasticity [dimensionless]
E	elliptic integral of the second kind for the elliptical paraboloid asperity [dimensionless]
E^*	combined elastic modulus of the contacting materials [Pa]
F	force [N]
H	hardness of the deforming material [Pa]
K	elliptic integral of the first kind for the elliptical paraboloid asperity [dimensionless]
K_v	contact pressure factor for the hardness of deforming material [dimensionless]
P_m	mean Hertzian contact pressure [Pa]
P_{nom}	nominal contact pressure [Pa]
R	radius of the elliptical paraboloid asperity [m]
S_q	root mean square of the surface roughness [m]
α	non dimensional semi-axis of contact ellipse in major direction [dimensionless]
β	non dimensional semi-axis of contact ellipse in minor direction [dimensionless]
γ	non dimensional interference of elliptical paraboloid [dimensionless]
δ	non dimensional interference of asperity, [dimensionless]
κ	ellipticity ratio of asperity [dimensionless]
λ	asperity curvature ratio [dimensionless]
μ	coefficient of friction [dimensionless]
υ	Poisson ratio [dimensionless]
φ	orientation of the elliptical paraboloid asperity with sliding direction [°]
σ_y	yield strength of the deforming material [Pa]
σ_κ	standard deviation of the asperity curvature [m^{-1}]
σ_s	standard deviation of the asperity slope [m^{-1}]
τ_{BL}	shear strength of boundary layer [Pa]
ψ	bandwidth parameter of surface [dimensionless]
ω	interference of asperity [m]

Subscript

1	transition point for interference from elastic to elastic–plastic deformation mode
2	transition point for interference from elastic–plastic to full plastic deformation mode
e	elastic deformation mode
ep	elastic–plastic deformation mode
p	fully plastic deformation mode
t	tool
wp	workpiece (sheet material)
x	major direction of elliptical paraboloid asperity
y	minor direction of elliptical paraboloid asperity
W	frictional force
N	normal force

Superscript

$'$	tool asperity
ul	unloading mode
$trans$	transition load/area at the onset of plasticity

However, the individual effects like normal loading, stretching and repeated contacts for surface deformation cannot be quantified. Strip drawing test has been used by ter Haar [7] to measure the effect of surface deformation (due to normal loading and pre-stretching) and sliding speed to construct a Stribeck curve for deep drawing process. The friction is found to be hardly influenced by the bulk deformation process. Roizard et al., [8] has also used a strip drawing test to measure the friction for sheet metal forming to study the influence of repeated contacts and temperature influence. They showed that the coefficient of friction in repeated contacts has increased due to adhesive transfer of material. Emmens [9] used a rotational friction tester to study the influence of surface roughness, lubrication and various material combinations only for normal loading conditions. Jonasson et al., [10] used a bending under tension test to measure the friction using different textured surfaces by replicating the deformation zone in die radius. Wiklund et al., [11] also used a bending under tension test to validate a friction model with normal loading, bulk deformation and lubrication effects for different surface textured sheet material at various sliding speed. There has been a wide variety of contact models have been developed as well as experiments have been conducted to understand the tribological behaviour in deep drawing process. The correlation between models and experiments is still lacking to understand the individual effects. This article focuses on improving the predictability of the developed friction models related to normal loading and reloading of surfaces. Bulk deformation adds complexity to the friction measurements in both the strip drawing test as well as bending under tension tests due to change in surface roughness and bending forces respectively. The contact models to predict the coefficient of friction described in [12–21] discusses the effects of asperity flattening due to normal loading and bulk deformation, ploughing, third body effects, boundary and mixed lubrication conditions. However, the deformation of the sheet surface is assumed to be rigid plastic. The current work focuses on improving the contact models for mixed modes of deformation for loading and reloading contact conditions.

1.2. Contact model

Tool and sheet material surfaces are nominally flat. When two nominally flat surfaces are brought into contact, the contact occurs only at certain spots as shown in Fig. 2. Hence, the real contact area is generally smaller than the nominal contact area. The contacting surfaces differ in roughness levels. The tool surface is generally smoother than the sheet material surface. In the contact model, it can be assumed that the tool is smooth at the workpiece (sheet material) roughness scale [12]. The smooth tool flattens the encountered workpiece asperities. The asperities undergo mixed modes of deformation when subjected to loading/reloading of surfaces. An elastic–plastic contact model from Jamari and Schipper [22] is used to describe the deformation of workpiece asperities for reloading contact conditions. At a smaller scale (i.e., tool roughness level), the tool asperities indent into the flattened workpiece. During sliding, the indented tool asperities plough through the workpiece. A tool indentation model for

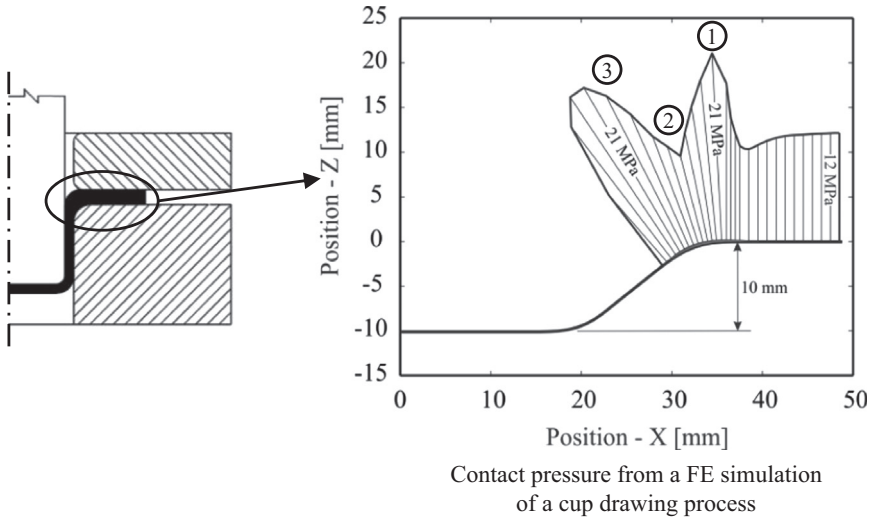

Fig. 1. Contact conditions from FE simulation of a deep drawing process.

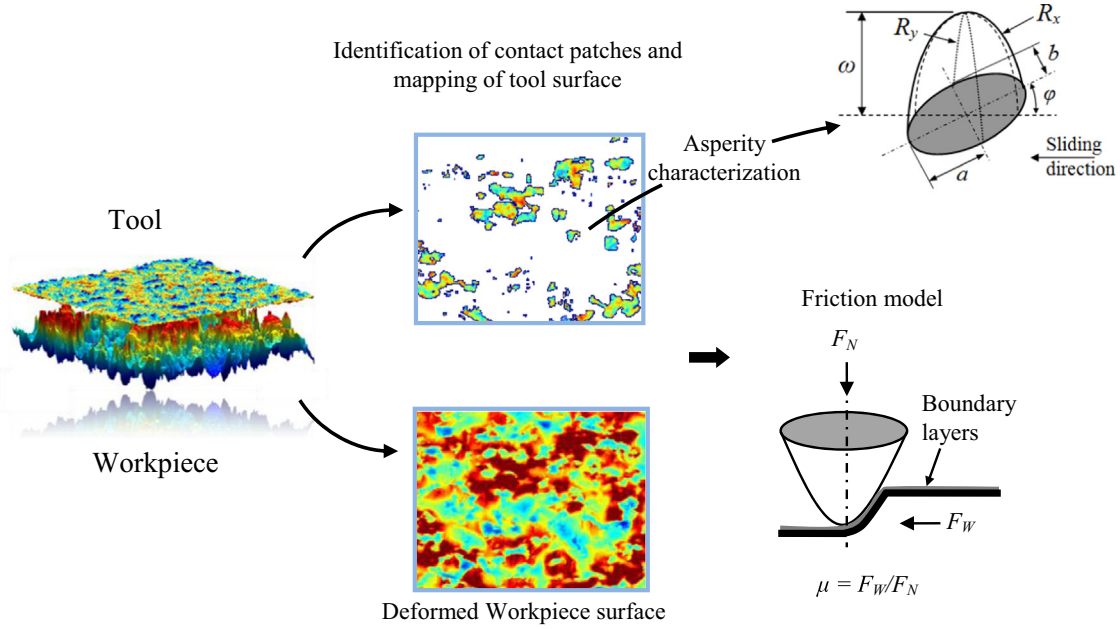

Fig. 2. Contact occurring between tool and sheet metal surfaces in deep drawing processes.

elastic–plastic contact is described by Masen et al., [23] to calculate the wear process. The coefficient of friction is calculated based on the ploughing of the tool asperities as described by Karupannasamy et al., [13] for two rough surfaces in contact using the model of [23].

1.3. Asperity characterization

The surface is represented in a height matrix of pixels. As the contact load is increased, the surface separation reduces. For a known surface separation, the contact patches are located within the height matrix. The contact patches are identified by means of connected pixels. After the contact patches are identified, they were characterized as elliptical paraboloids using the volume and area of the contact patch as given by de Rooij et al. [24]. This gives a better control for the description of the asperity compared to the conical or spherical shape according to [14,23,24]. The base area of the contact patch is described using an ellipse with a semi-major and semi-minor radii, a and b and the orientation of the ellipse with respect to sliding direction, φ as shown in Fig. 2. The elliptical paraboloid asperity is characterized with radii in the major and minor axis directions as denoted by R_x and R_y.

2. Single asperity deformation model

An asperity which is in contact undergoes three different modes of deformation with increasing load, i.e. elastic, elastic–plastic and plastic deformation. When the load is increased to a critical load which is beyond the elastic regime, the onset of plasticity occurs. The plasticity occurs beneath the surface. While unloading the asperity, a part of the deformation zone remains plastic and the rest of the deformation recovers. The asperity geometry changes due to the plastic deformation. A finite element simulation is shown by Shankar and Mayuram [25] for the deformation of hemispherical asperity with a rigid flat. Initially, a plastic deformation zone starts in a small

contained region just beneath the centre of the asperity. The condition at the very apex of the asperity is a hydrostatic stress state since the pressure is infinite. The plastic deformation zone is surrounded by a hydrostatic core and the elastically deforming region as shown by Johnson [26]. With a further increase of load, the plastic region between the hydrostatic core and the elastic region grows. When a full plastic deformation stage is reached, the core and the elastic region are enveloped by the plastic region. A lot of attention has been paid to the contact model for the mixed modes of deformation at single asperity level [27–29].

2.1. Asperity loading

The asperity loading model for an elliptical paraboloid asperity is presented in this section according to [30].

2.1.1. Elastic contact

From Hertz's theory of elasticity, the elastic contact area and load are expressed in terms of interference of the asperity and its geometry. The elastic contact area, A_e for an elliptical paraboloid is given as

$$A_e = 2\pi R\frac{\alpha\beta}{\gamma}\omega \tag{1}$$

The mean effective radius, R of the asperity is given as

$$\frac{1}{R} = \frac{1}{R_x} + \frac{1}{R_y} \tag{2}$$

The dimensionless parameters for the elastic contact situations are given as [30]

$$\alpha = \kappa^{1/3}\left[\frac{2}{\pi}E(m)\right]^{1/3} \tag{3}$$

$$\beta = \kappa^{-2/3}\left[\frac{2}{\pi}E(m)\right]^{1/3} \tag{4}$$

$$\gamma = \kappa^{2/3}\left[\frac{2}{\pi}E(m)\right]^{-1/3}\frac{2}{\pi}K(m) \tag{5}$$

The elliptic integrals $E(m)$ and $K(m)$ are approximated as

$$E(m) \approx \frac{\pi}{2}(1-m)\left[1+\frac{2m}{\pi(1-m)}-0.125\ln(1-m)\right] \tag{6}$$

$$K(m) \approx \frac{\pi}{2}(1-m)\left[1+\frac{2m}{\pi(1-m)}\ln\left(\frac{4}{\sqrt{1-m}}\right)-0.375\ln(1-m)\right] \tag{7}$$

where

$$m = 1-\kappa^2 \tag{8}$$

$$\kappa = \left[1+\sqrt{\frac{\ln(16/\lambda)}{2\lambda}}-\sqrt{\ln 4}+0.16\ln\lambda\right]^{-1} \quad \text{for } 0<\lambda\le 1 \tag{9}$$

The asperity curvature ratio is defined as

$$\lambda = \frac{R_x}{R_y} \tag{10}$$

The contact load carried by an elliptical paraboloid asperity under elastic conditions is given as

$$F_{N,e} = \frac{4}{3}E^*\left(\frac{\omega}{\gamma}\right)^{3/2}\sqrt{2R} \tag{11}$$

The critical interference at which the onset of plasticity occurs for the given asperity geometry and material properties is calculated from the Hertzian contact theory. The mean contact pressure for the Hertzian contact of an elliptical paraboloid is given as

$$P_m = \frac{F_{N,e}}{A_e} = \frac{2\sqrt{2}}{3\pi}\frac{E^*}{\alpha\beta}\left(\frac{\omega}{R\gamma}\right)^{0.5} \tag{12}$$

The full plastic deformation initiates when the mean Hertzian contact pressure exceeds a contact pressure factor according to Tabor [2]. The contact pressure factor is related to hardness of the material and a hardness coefficient.

$$P_m = K_v H \tag{13}$$

The hardness coefficient related to Poisson's ratio of the material from the von Mises shear strain energy criterion according to [31] is given as

$$K_v = 0.4645+0.3141\nu+0.1943\nu^2 \tag{14}$$

The critical interference for the onset of plasticity is given from Eqs. (12)–(14),

$$\omega_1 = \frac{\pi^2}{2}(\alpha\beta)^2\gamma R\left(\frac{K_v H}{E^*}\right)^2 \tag{15}$$

2.1.2. Full plastic contact

In the fully plastic regime, the contact pressure carried by the asperity is equal to the hardness of the material. Then, the contact load and area of the plastically deforming asperity is obtained by simply truncating the asperity geometry as described by Abbott and Firestone [32]. The contact area of the elliptical paraboloid asperity under full plastic conditions is given as

$$A_p = 2\pi\sqrt{R_x R_y}\omega \tag{16}$$

The plastic load under contact is given as

$$F_{N,p} = 2\pi\sqrt{R_x R_y}\omega H \tag{17}$$

An accurate description for the interference to achieve full plastic deformation is not known. It is estimated by using Johnson's criteria for full plastic deformation. According to Johnson [26], full plastic deformation occurs when the contact load equals 400 times the load at first plastic yielding. The contact load at first yielding is calculated by assuming again that the mean contact pressure equals the hardness of the material.

$$\frac{F_{N,p}^{trans}}{F_{N,e}^{trans}} = \frac{2\pi\sqrt{R_x R_y}\omega_2 H}{2\pi R\alpha\beta\gamma^{-1}\omega_1 K_v H} = 400 \tag{18}$$

After solving Eq. (18), the transition interference for the full plastic deformation is given as

$$\omega_2 = C_A\frac{\sqrt{\lambda}}{1+\lambda}\frac{1}{\kappa}\frac{E(m)}{K(m)}\omega_1 \tag{19}$$

The parameter C_A is the ratio of contact area to the critical contact area for the first plastic yield. For steel, the value for $C_A = 160$ by Jackson and Green [33].

For spherical steel contacts ($\lambda = 1$), the transition can be further simplified as,

$$\omega_2 = 80\omega_1 \tag{20}$$

2.1.3. Elastic–plastic contact

Zhao et al., [29] proposed an elastic–plastic contact model (ZMC model) by providing a smooth transition between the elastic and plastic contact areas. In the elastic–plastic deformation mode, the contact area changes from a complete elliptic area to a semi-elliptic area. Zhao et al., used a cubic polynomial expression using the transition interference to join the two asymptotes for the

contact area. The relative interference is given as

$$\delta = \frac{\omega - \omega_1}{\omega_2 - \omega_1} \tag{21}$$

The contact area during elastic–plastic deformation after scaling is given as

$$A_{ep} = A_e + (A_p - A_e)(-2\delta^3 + 3\delta^2) \tag{22}$$

The elastic–plastic contact load is obtained from the mean contact pressure and the contact area during elastic–plastic deformation as

$$F_{N,ep} = A_{ep}\left[H - H\left(1 - \frac{2}{3}K_v\right)\frac{\ln \omega_2 - \ln \omega}{\ln \omega_2 - \ln \omega_1}\right] \tag{23}$$

2.2. Unloading of single asperity contact

In deep drawing processes, the coefficient of friction is not only influenced by loading of surfaces but also during repeated loading cases. When an asperity deforms at a contact pressure and again subjected to reloading at a lower contact pressure, the asperity is expected to deform elastically as the plastic deformation has already happened in the first loading stage. This will influence the contact area and contact load carried by the deforming asperity. In the elastic deformation mode, the contact load carried is less than the plastic load. Since the friction is majorly influenced by contact area, it is in fact the main focus to incorporate reloading effects. The asperity geometry will change after unloading depending on the deformation mode as shown in Fig. 3. The residual interference and radius of the asperity have been changed after the initiation of plastic deformation.

2.2.1. Elastic unloading

During elastic deformation of an asperity, the contact area and load are calculated according to the Hertzian theory. Once when the contact load is removed, the asperity deformation is completely reversible as shown in Fig. 3(a). During reloading, the asperity remains elastic and still deforms in the same mode. While unloading the asperity, the residual interference and asperity geometry remains unchanged.

$$\omega_{ul,e} = \omega;\ A_{ul} = 0;\ R_{ul,e} = R \tag{24}$$

2.2.2. Elastic–plastic unloading

During unloading of elastic–plastic contact, a significant amount of elastic recovery takes place depending on the degree of plastic deformation. The residual geometry and interference are also changed during the unloading process as shown in Fig. 3(c). When the asperity is removed from the load, the plastic deformation has already happened. When reloaded to the same contact load, it is assumed that the whole deformation process is completely elastic. Hence, the contact load and contact area is given as,

$$F_{N,ep} = \frac{4}{3}E^*\left(\frac{\omega_{ul,ep}}{\gamma}\right)^{3/2}\sqrt{2R_{ul,ep}} \tag{25}$$

$$A_{ep} = 2\pi R_{ul,ep}\frac{\alpha\beta}{\gamma}\omega_{ul,ep} \tag{26}$$

The deformed asperity geometry after unloading is calculated from the elastic laws and keeping the original asperity curvature ratio and contact area. The residual radius, $R_{ul,ep}$ and residual interference, $\omega_{ul,ep}$ is calculated by solving the two Eqs. (25) and (26).

2.2.3. Fully plastic unloading

During unloading of plastic deformation mode, the elastic recovery of the asperity is small. Even though the residual interference of the asperity is small, the residual radius of the asperity becomes very large as shown in Fig. 3(b). The change of the residual radius cannot be neglected while reloading. During reloading of the asperity, the load and the contact area should be according to the elastic deformation mode when the previous plasticity is not exceeded. The residual radius and interference are found by satisfying the elastic deformation laws. In the analysis, the asperity curvature ratio is kept constant. The residual radius $R_{ul,p}$ and interference, $\omega_{ul,p}$ are found from the contact area and load for the elastic contact by solving the two Eqs. (27) and (28).

$$F_{N,p} = \frac{4}{3}E^*\left(\frac{\omega_{ul,p}}{\gamma}\right)^{3/2}\sqrt{2R_{ul,p}} \tag{27}$$

$$A_p = 2\pi R_{ul,p}\frac{\alpha\beta}{\gamma}\omega_{ul,p} \tag{28}$$

3. Elastic–plastic ploughing model

The friction between the surfaces is caused by interfacial shear and ploughing in micro-contacts during sliding. For friction modelling, the geometry of the indented tool asperities into the deformed contact patches of the workpiece is important. With the indented geometry of the tool asperity, the coefficient of friction can be calculated using Challen and Oxley's model [34] for ploughing and cutting deformation modes with an interfacial friction factor. Under complete elastic conditions, the asperity indents and the material fully recovers after the indenter passed as shown in Fig. 4. In the elastic–plastic contact situations, the frontal part of the asperity carries the tangential load during sliding. The contact area changes from a complete elliptic area to a semi-elliptic area according to Masen et al. [23]. For fully plastic conditions, the asperity indents and there is no elastic recovery after the indenter has passed.

Only the front half of the asperity will be in contact during ploughing in fully plastic regime. In elastic–plastic situations, there is elastic recovery depending on the degree of plasticity. The contact pressure and contact area follow from the asperity geometry for the given indentation depth. When there is a plastic deformation, the total deformation is permanent and the contact pressure equals the indentation hardness of the material. The indentation hardness is size and shape dependent. For an elliptical

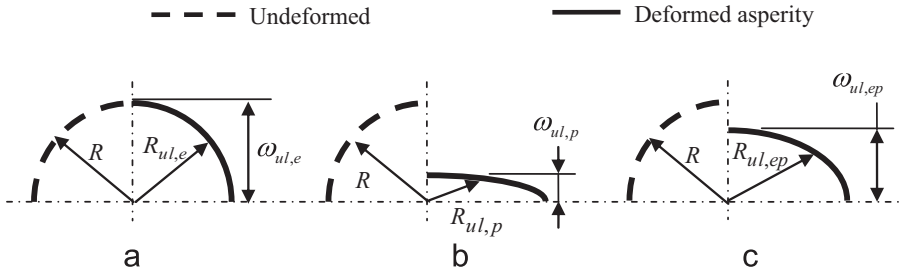

Fig. 3. Representation of asperity deformation for (a) elastic (b) fully plastic and (c) elastic–plastic after unloading.

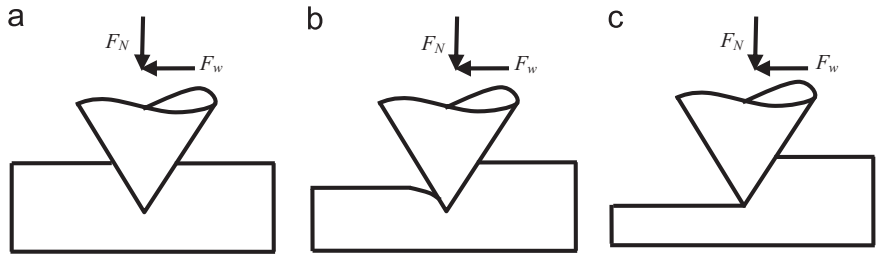

Fig. 4. Indentation of tool asperity at (a) elastic (b) elastic–plastic and (c) fully plastic deformation modes.

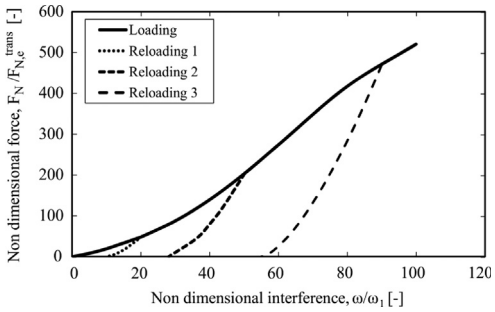

Fig. 5. Calculated force displacement curve for loading/reloading for a single asperity contact with a rigid flat for mixed modes of deformation.

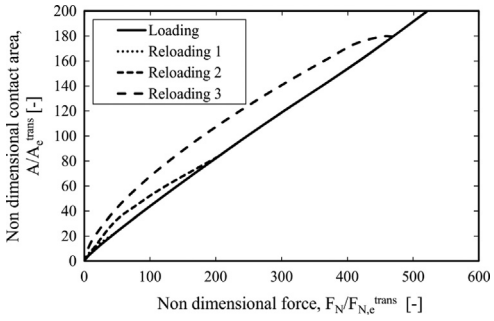

Fig. 6. Calculated force area relation for loading/reloading for a single asperity contact with a rigid flat for mixed modes of deformation.

paraboloid asperity, the contact area under ploughing conditions assuming only front half of the asperity makes contact is given as

$$A_t = \pi\sqrt{R'_x R'_y}\,\omega' \tag{29}$$

The contact load for indentation at fully plastic conditions is given as,

$$F_{N,t} = HA_t \tag{30}$$

Similar to the flattening model, the contact load and area for an asperity is calculated for elastic and elastic–plastic deformation with the Eqs. (1), (11), (22) and (23). The transition points from elastic to fully plastic conditions are found with the Eqs. (15) and (20).

4. Reloading of single asperity contact

A large amount of sliding takes place in the blank holder region during deep drawing of the sheet material, where loading/reloading of the surface takes place. A single asperity contact model is shown in this section for loading/reloading conditions with a rigid flat contact.

During the first loading, the asperity will undergo different modes of deformation. With the subsequent loading at the same contact load, the asperity deformation is assumed to be elastic provided that there are no running-in effects. The numerical results of the loading and reloading process are shown in Figs. 5 and 6. The force-displacement during loading is calculated according to the mode of deformation as explained in Section 2. and the reloading relation is calculated from the elastic deformation mode as explained in Section 2.2. Fig. 5 shows the plot of non-dimensional interference and non-dimensional load. The interference and load is normalized by their critical values at which the transition from elastic to plastic regime starts. Non-dimensional interference, $\omega/\omega_1 = 1$ means that plastic deformation starts, where the reloading behaviour is different from the loading process. The reloading relation for different reloading cycles (reloading 1, 2 and 3) have the same slope i.e., contact

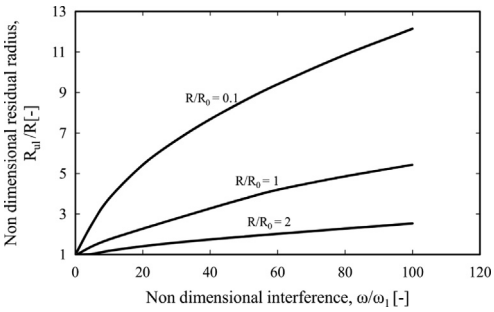

Fig. 7. Calculated residual radius for a given interference after unloading of the single asperity contact with a rigid flat.

stiffness. The reloading curve is non-linear for elastic deformations which is similar to the indentation experiments on micro and nano scale indentations by Oliver and Pharr [35,36]. One important observation from the indentation experiments is that the shape of the indentation after reloading is different and the material recovers elastically. The impression with the spherical indentation in metals resulted with a larger radius than the indenter. This phenomenon is also observed in the asperity flattening model when calculating the residual geometry shape. During the experiments, the material is loaded and unloaded a few times before the force-displacement behaviour becomes completely reversible. Limited amount of plasticity occurs in few loading cycles. This can be due to material creep during loading and reloading cycles.

In Fig. 6, the contact area development is shown during loading and reloading for a sphere of radius 10 μm. The original curvature ratio of the asperity is assumed to be unchanged during elastic recovery. While reloading at same load, the contact area is larger than during the loading. This is due to the fact that the asperity radius became larger during unloading due to elastic conditions which is also in agreement the indentation experiments [35].

In Fig. 7, the change of contact radius is shown during the loading process. For elastic deformation i.e. $0 < \omega/\omega_1 < 1$, the residual remains unchanged. As the plasticity progresses with the increased load, the asperity radius increases which was also

observed in indentation experiments of [35,36]. The asperity radius continues to increase with the contact load and becomes flattened with a larger radius. In practice, the asperity radius reaches infinite for large plastic deformation conditions. Next, the influence of the asperity radius is compared in the figure. The reference radius of the asperity, R_0, is taken as 10 μm. When the asperity radius is small ($R/R_0=0.1$), there is more plastic deformation as the smaller asperities deforms plastically due to high contact pressure. When the asperity radius is high ($R/R_0=2$), the asperity deforms more in the elastic–plastic regime and the elastic recovery is higher. The residual radius will be much closer to the original radius of the asperity after unloading. The asperity radius continues to increase with the contact load and becomes completely flattened with a larger radius when full plasticity deformation is achieved.

5. Contact analysis of numerically generated rough surfaces

Depending on the shape and size of the asperities, the deformation may operate in the three different modes of deformation. In this section, the contact model is subjected to the analysis of how the contact pressure and surface roughness influences the transition from elastic to fully plastic deformation for multi-asperity contacts. For this analysis, the surfaces are numerically generated by using the fast Fourier techniques of Hu and Tonder [37]. In Fig. 8, the influence of the contact pressure is shown on the transition of the asperity deformation from elastic to fully plastic deformation. The non-dimensional indentation depth is the ratio of the indentation depth, ω' to the contact radius of the elliptical base. The non-dimensional indentation depth can be small either due to the smaller asperity deformation or larger asperity contact radius. The asperity deforms solely or partly in an elastic manner at small deformations. As the non-dimensional indentation depth increases, the asperity deforms more in the plastic regime. From the plot, it can be seen that the deformation of surface cannot be considered to operate only in the fully plastic mode as considered in [4–6,12]. When the contact pressure is increased the number of asperities in contact also increases and also they merge together to form bigger contact patches. As a result, the non-dimensional indentation depth of the asperity decreases. The bigger asperities operate in the elastic–plastic deformation mode while the smaller asperities undergo fully plastic deformation. Although the number of asperities operate in fully plastic deformation mode is large, the major percentage of the total load is carried by large asperities operating in elastic–plastic mode increases with the increase in nominal contact pressure as shown in Fig. 8. The percentage of the load carried by the pure elastic mode is negligible in this analysis.

The surface roughness indicates how the shape of the asperities is distributed. If the surface is rough, the asperities are sharp. In Fig. 9, the influence of surface roughness on the asperity deformation mode is shown. The surfaces are generated with a different roughness with constant auto-correlation length. If the surface is smooth, the number of asperities in contact is high. The asperities undergo mixed modes of deformation. The majority of the asperities operate in the elastic–plastic mode. When the surface roughness increases, the elastic–plastic deformation of the asperities are diminishing. For the roughest surface ($S_q=0.4$ μm), there are a large number of asperities in plastic mode of deformation.

6. Loading/reloading analysis on sheet metal surface

The single asperity loading/reloading model explained in the previous section is used in a multi-asperity contact situation. A typical surface from DC06 sheet material and a tool surface are used for the reloading analysis as shown in Appendix A (see Figs. A1 and A2). The asperities are characterized by elliptical paraboloids for the given load as described in Section 1.3. In Fig. 10,

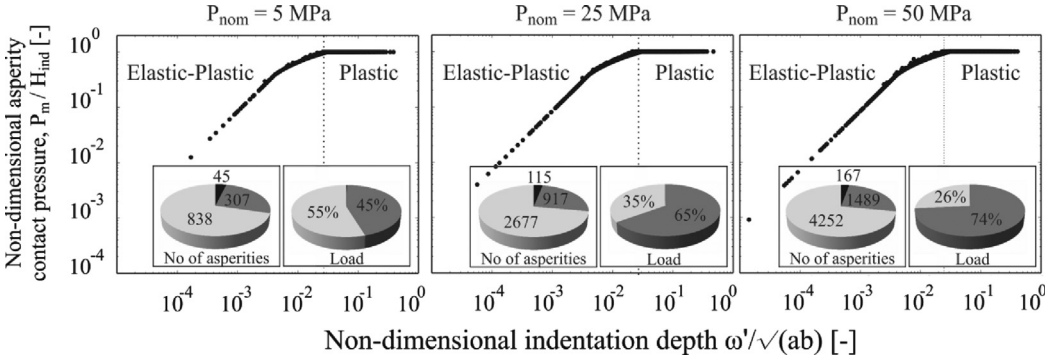

Fig. 8. Influence of contact pressure on asperity deformation mode (■ – Elastic, ■ – Elastic–plastic, ■ – Plastic).

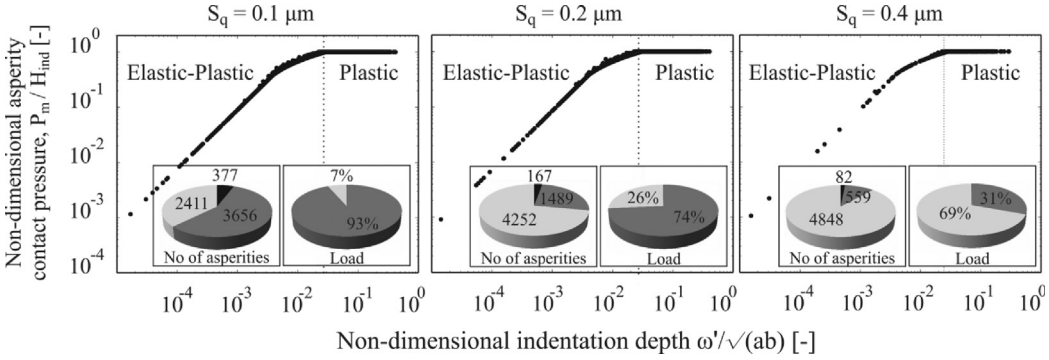

Fig. 9. Influence of surface roughness on the asperity deformation mode (■ – Elastic, ■ – Elastic–plastic, ■ – Plastic).

the development of the nominal contact pressure is shown as a function of surface separation. At the beginning of the approach (i.e., high surface separation), only few asperities are in contact and the load is low. When the surface separation is decreased further, large number of asperities comes into contact and therefore the contact pressure increases rapidly. When the surface is reloaded to a lower contact pressure than the previous contact pressure, the asperities deforms in the elastic deformation mode. The contact pressure and fractional contact area are calculated for reloading cycles (Reloading 1 and 2) for the elastic deformation mode as shown in Figs. 10 and 11.

The fractional contact area during loading and reloading is shown in Fig. 11. During loading, the contact area increases as the surface separation decreases. When the surface is reloaded, the contact area is larger as the asperities are elastically deforming (shown for the single asperity contact, see Fig. 6). The fractional contact area during reloading cycles (Reloading 1 and 2) will increase steeply if there is a large plastic deformation of the surface during the initial loading. Smaller asperities undergo complete plastic deformation since the contact pressures are high. Larger asperities undergo elastic–plastic deformation and a considerable part of the asperity deformation is recovered.

The plot of the contact area of the asperities is shown for the given DC06 surface in Fig. 12. The contact area development is shown for contact pressures of $P_{nom}=5$, 25 and 50 MPa. For reloading, the surface is first subjected to a maximum contact pressure of $P_{nom}=50$ MPa and reloaded to lower pressures ($P_{nom}=5$ and 25 MPa). During loading, the bigger contact patches undergoes elastic–plastic deformation, while some smaller contact patches undergoes plastic deformation. It can be seen that the smaller contact patches are not found during the reloading at the same contact pressures (i.e., $P_{nom}=5$ and 25 MPa) when compared with the first loading. This is due to large amount of plastic deformation experienced by smaller asperities. The residual interference of these smaller asperities is apparently lower than the surface separation during the reloading conditions. Meanwhile, the large contact patches shows increased contact area during reloading at $P_{nom}=5$, 25 MPa. The contact area of the major contact patches while reloading are larger than at the first loading.

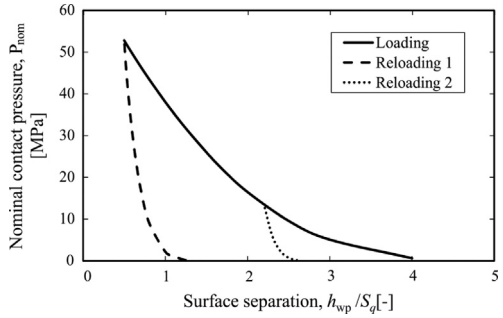

Fig. 10. Loading/reloading of surfaces using multi-asperity contact model.

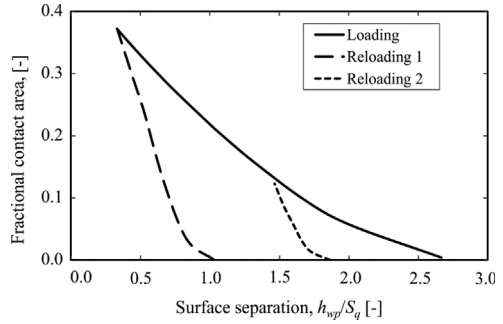

Fig. 11. Fractional contact area as a function of surface separation.

7. Influence of interfacial friction

The calculated coefficient of friction from the asperity deformation and indentation model is discussed in this section. The effect of shear stress between the contacting surfaces is usually expressed by the interfacial friction factor, f_{hk}. The friction factor is dependent on the properties of the boundary layers formed on the surface and the indenter geometry. The friction factor is defined as the ratio of the local shear strength to the shear strength of the deforming material. The local shear strength is dominated by the boundary layers if the contacting surface is flat (i.e. no ploughing). While ploughing, there is a rupture of the boundary layers and it degrades at the local asperity scale. Torrance et al. [38] accounted for the degradation of the boundary layers by adding a term called the fractional defect of the boundary layers, f_d. The interfacial friction factor at the interface is given as

$$f_{hk}=\frac{\tau_{BL}(1-f_d)+kf_d}{k} \tag{31}$$

The friction factor $f_{hk}=1$ means that there are no boundary layers and the surface is chemically clean. The shear strength of the surface is equal to the shear strength of the bulk material. Kopalinsky and Black [39] studied the influence of metallic sliding during indentation. The experiment was done using a hard wedge, representing an up-scaled asperity under boundary lubricated conditions. The main objective of the experiment is to study the effect of forces and stresses in wave-wedge formation from initial indentation to steady state sliding. They estimated the friction factor to be around $f_{hk}=0.68$ for wedge indentation using slipline analysis. Hokkirigawa and Kato's [40] experiments on steel also show that the interfacial friction factor for ploughing and cutting modes are between 0.5 and 0.9 depending on the degree of penetration. This shows that the boundary layer properties are degraded under the local asperity conditions. The influence of the degradation factor on the coefficient of friction is shown in Fig. 13 for the contact between two surfaces. The coefficient of friction is calculated for three different rough surfaces of DC06 sheet material (see Fig. A.1 in Appendix A). The error bar shows the variation due to the surface measurements made at different spots of the same sheet material surface. To achieve the high friction factor estimated by [38,39] for local asperity conditions, the degradation factor (f_d) can be in the range of 0.5–0.7. The coefficient of friction increases with degradation of the boundary layers as shown in Fig. 13.

8. Evolution of friction conditions during reloading of surfaces

The coefficient of friction is calculated with the asperity deformation model presented in this article and the ploughing model as explained by Masen et al., [23]. Challen and Oxley's model [34] is used to calculate the friction for the single asperity. The model is based on the slipline analysis of the 2D wedges. Hokkirigawa and Kato [40] conducted experiments and corrected the slipline model with correction factors for 3D asperity shapes. An elaborate description of the contact and the friction model for fully plastic contact conditions is given in [13]. The same approach has been used with the extension to elastic–plastic conditions for the contact between two surfaces. The coefficient of friction during loading and reloading is obtained with the contact models as shown in Fig. 14. During the first loading cycle, the coefficient of

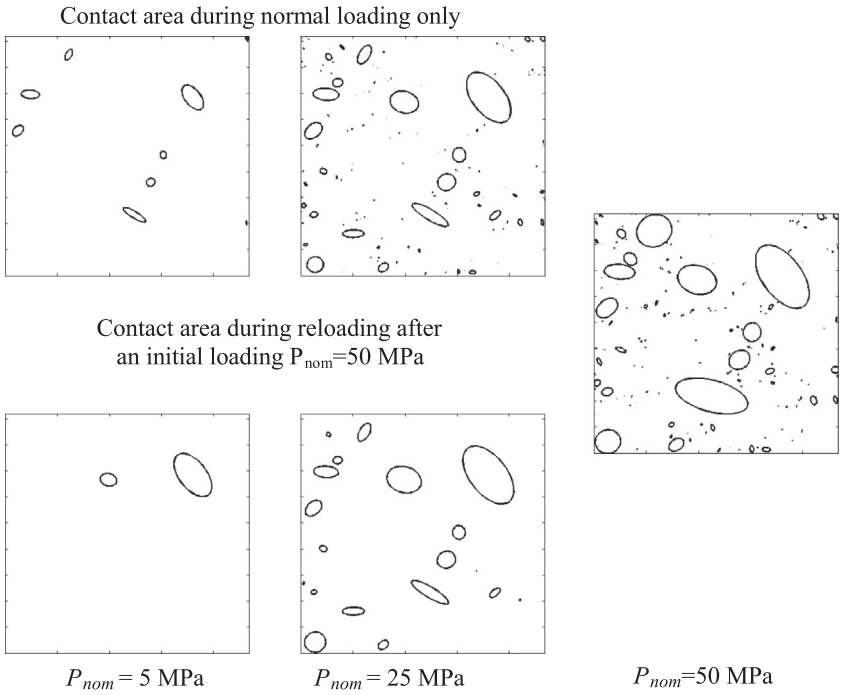

Fig. 12. Contact area development for the surface during loading/reloading for a maximum P_{nom}=50 MPa.

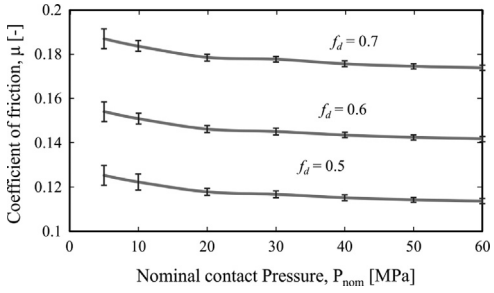

Fig. 13. Influence of boundary layer degradation.

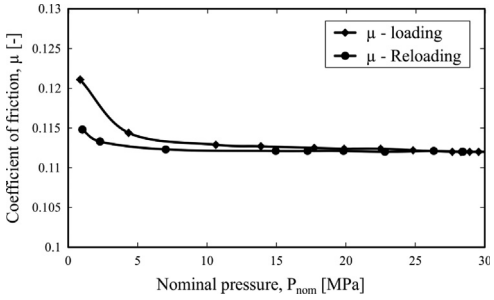

Fig. 14. Development of coefficient of friction for the reloading cycles with different nominal pressures.

friction decreases with the increase of contact pressure. When the indentation is increased, the asperities cluster together and forms blunt contact patches which results in decrease of friction. This trend of friction is dominant for the deformation dependent mechanism, i.e., ploughing.

During the first loading cycle, the contact area between the surfaces is already established. In this calculation, the surface is preloaded with nominal pressure of 30 MPa and reloaded with lower contact pressures. During reloading for the same lower contact pressures, the larger contact area is formed. This results in again clustering of the asperities due to the increase of contact area which further reduces the coefficient of friction. For the same maximum contact pressure as the initial loading pressure (P_{nom}=30 MPa), there is no difference in the friction.

9. Experimental validation

The developed contact model is compared with the experimental results in this section. The experiments are performed under laboratory conditions since the friction at the local contact conditions is difficult to measure in the actual deep drawing processes. In the actual deep drawing operation, sheet material is pulled over the die. The friction tester simulates the same condition by sliding the sheet material over the stationary tool with constant nominal contact pressure and sliding velocity. The friction model calculates the coefficient of friction with the measured workpiece and tool surfaces, material properties of the sheet material and given contact pressure. The experiments are performed in the boundary lubrication regime. Finally, the measured friction values are compared with the calculated values to check the validity of the friction model.

9.1. Experimental setup

The rotational friction tester (RFT) developed at Tata Steel is used to measure the coefficient of friction which occurs between the sheet and tool material. A schematic representation of the friction tester is shown in Fig. 15. The RFT can be used in different ways to study the friction dependency on various contact pressures, sliding conditions and lubrication conditions. The RFT consists of a rotating platform where the sheet material material is placed. The tool is represented by three flat notches which contact the rotating sheet material with a hydraulic actuator. Three flat notches are machined to the same height level, which ensures that the pressure is evenly distributed over the three notches. The allowable deviation should be smaller than the surface roughness of the sheet material. For this purpose, notches are carefully polished. The contact pressure can be varied by the choice of notch sizes and hydraulic pressure. The

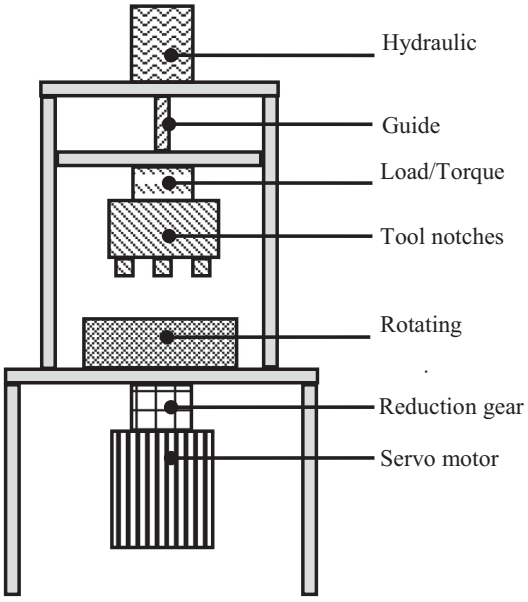

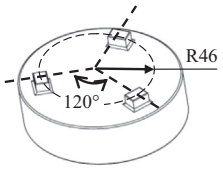

RFT Tool

Rotational frictional tester	
Pressure	5-60 MPa
Sliding velocity	10 mm/s
Mean contact area of notch	52.3mm^2
Mean radius of notch centre	46 mm

Fig. 15. Schematic representation of Rotational friction tester.

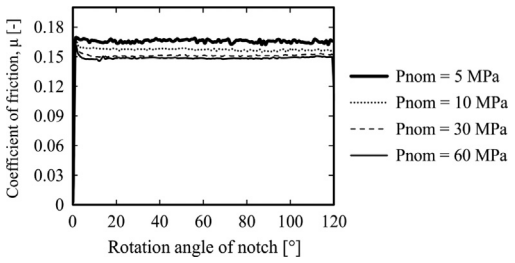

Fig. 16. Typical friction measurement for different nominal pressure from RFT.

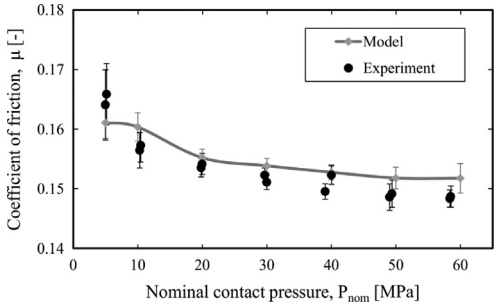

Fig. 17. Comparison of the coefficient of friction with the experiment and model.

elastic deformation of the tool is reduced by making the punches relatively thick and stiff. A computer controlled, brushless servo motor with low inertia reduction gear drives the specimen holder, which allows a greater flexibility for position and speed control.

9.1.1. Sheet material specimen

The sheet material material chosen here is uncoated DC06 EDT (Electrical discharged textured) cold rolled steel material which is typically used for deep drawing processes in the automotive industry. The sheet material is cut to a size of 120 × 120 mm^2 and cleaned with acetone and alcohol to remove any surface contaminants. A typical deep drawing oil, Quaker N6130, is applied on the sheet material surface. This lubricant is a conservation oil with deep drawing lubrication properties. The experiments are performed at room temperature conditions. The lubricant has a dynamic viscosity of 55 mPa s at 22 °C. The lubricant is controlled to an amount of 0.6 g/m^2 during oiling of the sheet material by using a mass balance. The sheet material specimen has a roughness in the order of S_q = 1.7 μm. The low amount of lubricant compared to the surface roughness and a relatively low sliding velocity indicates that there will be no hydrodynamic lubrication effects. The experiments are therefore performed in the boundary lubrication regime.

9.1.2. Tool specimen

The tool is made of three square notches made from uncoated tool steel material of grade DIN 1.2510. The notches are finely ground to a roughness, S_q = 0.08 μm by a lapping process so that there is a complete contact with the sheet material. The tool is supported in a central pivot system which will ensure uniform distribution of the load. The dimensions of the square notches are 8 × 8 mm^2. The notches are placed at a regular interval of 120° in a circular pattern of mean radius 46 mm to the centre of the notch.

9.1.3. Testing procedure

The lubricated sheet material is placed on the rotating platform and clamped firmly. The tool specimen comes into contact with the sheet material and the pressure is applied by the hydraulic actuator system. The nominal contact pressure between the sheet material and tool is applied in the range of 5–60 MPa. The applied load and frictional torque is measured by means of transducers. The sliding velocity of the rotational friction tester is kept constant at 10 mm/s. Before the test, the tools are cleaned to remove any lubricant present. Experiments are performed in triplicate to measure the variation within the tests. A typical measurement for the coefficient of friction is shown in Fig. 16. The figure shows the measured coefficient of friction for a rotational movement of 120°. The coefficient of friction remains constant over the sliding distance, except for the initial static friction which is higher.

9.2. Results

The mean coefficient of friction is obtained for various contact pressures using the RFT as shown in Fig. 17. The mean coefficient

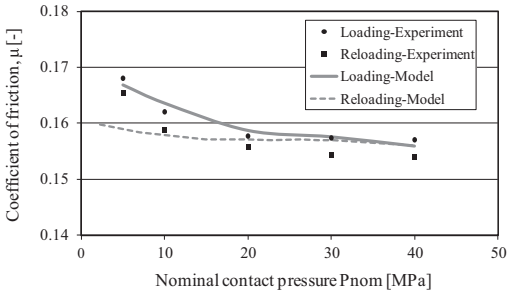

Fig. 18. Experiments on loading and reloading of surfaces.

of friction is calculated within the rotation angle of 20–100° to neglect initial static friction and tail end measurement errors. The coefficient of friction has been also calculated using the contact model as explained before for three different measured surfaces of DC06 sheet material and measured RFT tool surfaces. The input material parameters for the contact model are given in Table A1. The measured surfaces are shown in Fig. A.1. The error bars shown in the calculated coefficient of friction indicates the variation with respect to the different sheet material and tool surfaces used. The interfacial friction factor is adjusted by the boundary degradation factor to correlate with the experimental results. The friction factor, f_{hk} at the local asperity is found to be 0.6 which is also reasonable from the single asperity results of [38–40] for ploughing and cutting modes of deformation (f_{hk}=0.5–0.9) in steel under boundary lubricated conditions. The model predicts the trend of the friction with the contact pressure which is in agreement with the experiments.

Also the experiments on loading/reloading of surfaces were conducted to see the effect on the coefficient of friction as shown in Fig. 18. First, the coefficient of friction measured for varying contact pressures without any preloads. For the second case, the surface is first subjected to a preload of P_{nom}=40 MPa and then reloaded with lower contact pressures. The coefficient of friction is further reduced with the contact pressure for the preloaded surfaces. This similar trend was predicted with the model as shown in the figure. The friction model correctly predicts the reduction in friction for reloading at lower contact pressure. Further, the friction is predicted to remain same when the preloaded contact pressure is reached, where as in the experiments is found to be reduced. This difference may be caused by the change of sheet material surface due to repeated ploughing effects.

10. Conclusion

A model is developed to describe the friction behaviour and deformation of surfaces for loading/reloading conditions. For this, an elastic–plastic single asperity contact model is developed and extended to a multi-asperity contact situation. During reloading of the asperities, the deformation is assumed to be completely elastic in the contact model. An elastic–plastic ploughing model and a friction model are used to calculate the coefficient of friction during sliding. The friction model includes the roughness of both tool and sheet material surface at two different scales. During loading, the coefficient of friction decreases with increase of contact pressure. When the surface is subjected to a maximum contact pressure and subjected to reloading at lower pressures (as in the case of repeated contacts in deep drawing processes), the coefficient of friction reduces further. The model is compared for loading/reloading conditions using a rotational friction tester for the typical materials used in deep drawing processes. The experiments are performed with low amount of lubricant and low sliding velocity to ensure that the system operates in boundary lubrication regime.

The main outcomes of the model and experimental validation are listed as follows:

- The contact model describes the deformation of sheet material surface for loading and reloading of surfaces under the normal loading conditions with mixed modes of deformation.
- The coefficient of friction is calculated from the geometrical shape of indented asperities using the measured surface topographies for workpiece and tool.
- The friction model shows good agreement with the experiments if an appropriate value for interfacial friction factor is used for boundary lubricated contacts.
- The effect of boundary layer degradation at the local contact conditions is found to be important in the model to predict the coefficient of friction. If the boundary layer degrades, the friction tends to increase.
- The contact model can be made better by including the effects of repeated ploughing of sheet material surfaces by the tool asperities (i.e., running-in effects).
- The boundary layer model is described by a simple factor which can be improved using a physically based adsorption and degradation model with influence of operational conditions.

Acknowledgements

This research was carried out under the Project number MC1.07289 in the framework of the Research Program of the Materials innovation institute, The Netherlands (www.m2i.nl).

Appendix A

Input data for the model (Table A1), (Figs. A1 and A2).

Table A.1
Input parameters for the asperity deformation model.

Parameters	Values
Elastic modulus, E [GPa]	210
Hardness, H [MPa]	450
Yield strength, σ_y [MPa]	160
Poisson's ratio, υ [dimensionless]	0.3
Shear strength, τ_{BL} [MPa] (see [41])	$3.94P_{nom}^{0.81}$

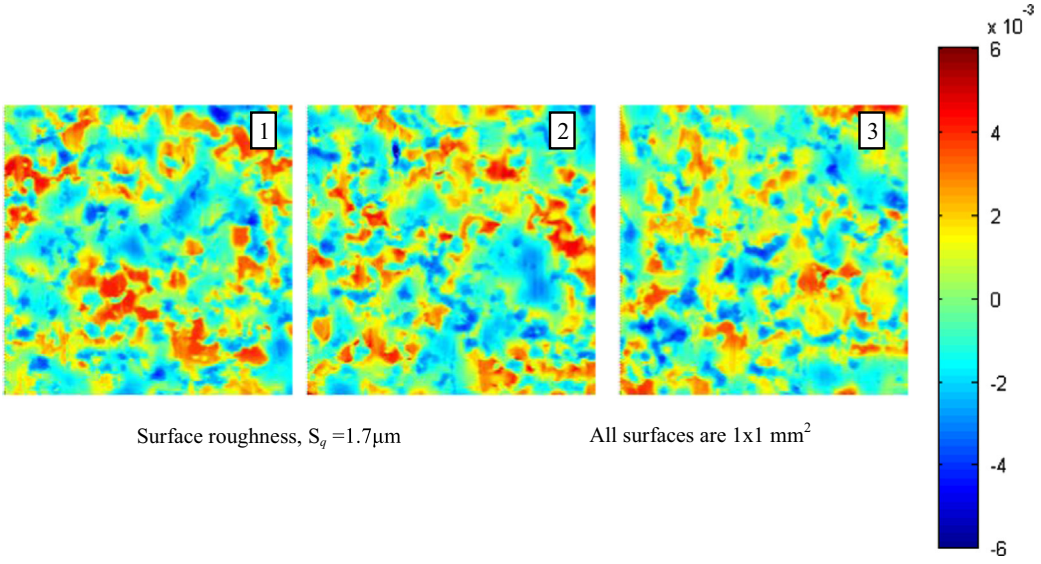

Fig. A1. Surface topography of the DC06 sheet material used in the experiments.

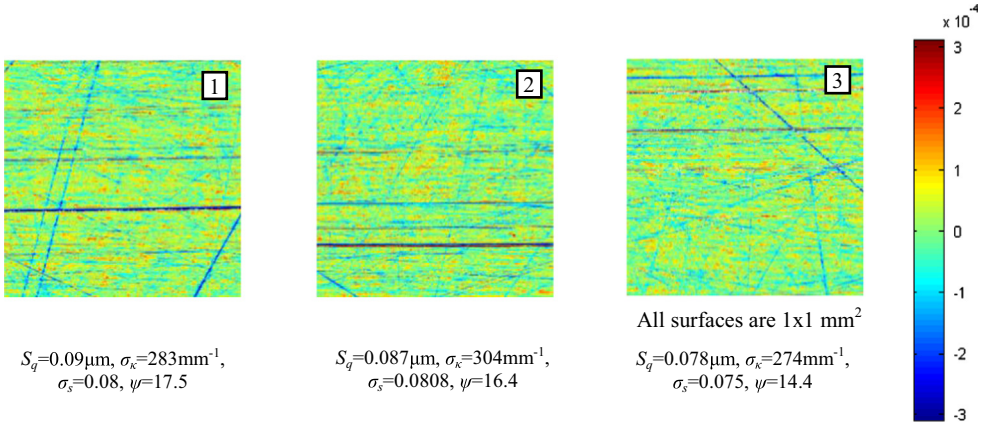

Fig. A2. Surface topography of the tool surface used in the experiments.

References

[1] M.P. Pereira, J.L. Duncan, W. Yan, B.F. Rolfe, Contact pressure evolution at the die radius in sheet metal stamping, J. Mater. Process. Technol. 209 (2009) 3532–3541.
[2] D. Tabor, The Hardness of Metals, Oxford University Press, UK, 1951 (isbn:0-19-850776-3).
[3] J.A. Greenwood, J.B.P. Williamson, Contact of nominally flat surfaces, Proc. R. Soc. Lond., Ser. A, Math. Phys. Sci. 295 (1966) 300–319.
[4] J. Pullen, J.B.P. Williamson, On the plastic contact of rough surfaces, Proc. R. Soc. Lond., Ser. A, Math. Phys. Sci. 327 (1972) 159–173.
[5] W.R.D. Wilson, S. Sheu, Real area of contact and boundary friction in metal forming, Int. J. Mech. Sci. 30 (1988) 475–489.
[6] M.P.F. Sutcliffe, Surface asperity deformation in metal forming processes, Int. J. Mech. Sci. 30 (1988) 847–868.
[7] R. ter Haar, Friction in sheet metal forming, the influence of (local) contact conditions and deformation (Ph.D. thesis), University of Twente, The Netherlands, 1996.
[8] X. Roizard, J.M. Pothier, J.Y. Hihn, G. Monteil, Experimental device for trbological measurement aspects in deep drawing process, J. Mater. Process. Technol. 209 (2009) 1220–1230.
[9] W.C. Emmens, Tribology of Flat contact and its application in deep drawing (Ph.D. thesis), University of Twente, The Netherlands, 1997 (ISBN: 90-365-1028-7).
[10] M. Jonasson, A. Wihlborg, L. Gunnarsson, Analysis of surface topography changes in steel sheet strips during bending under friction test, Int. J. Mach. Tools Manuf. 38 (1998) 459–467.
[11] D. Wiklund, B.G. Rosen, A. Wihlborg, A friction model evaluated with results from a bending under tension test, Tribol. Int. 42 (2009) 1448–1452.
[12] A. Westeneng, Modelling of contact and friction in deep drawing processes (Ph.D. thesis), University of Twente, The Netherlands, 2001 (ISBN: 90-365-1549-1).
[13] D.K. Karupannasamy, M.B. de Rooij and D.J. Schipper, Deterministic model for ploughing under rough contacts, in: 15th Nordic Symposium on Tribology-Nordtrib, Trondheim, Norway, ISBN 978-82-14-05270-1, 2012.
[14] X. Ma, M.B. de Rooij, D.J. Schipper, A load dependent friction model for fully plastic contact conditions, Wear 269 (2010) 790–796.
[15] J. Hol, M.V. Cid Alfaro, M.B. de Rooij, T. Meinders, Advanced friction modeling for sheet metal forming, Wear 286–287 (2012) 66–78.
[16] D.K. Karupannasamy, J. Hol, M.B. de Rooij, T. Meinders, D.J. Schipper, Modelling mixed lubrication for deep drawing processes, Wear 294–295 (2012) 296–304.
[17] W.R.D. Wilson, Friction models for metal forming in the boundary lubrication regime, J. Eng. Mater. Technol. 113 (1989) 60–68.
[18] D.K. Karupannasamy, M.B. de Rooij, D.J. Schipper, Multi-scale friction modelling for rough contacts under sliding conditions, Wear 308 (2013) 222–231.
[19] M. Janjic, V. Domazetovic, M. Vukcevic, Experimental-numerical friction factor determination, Tribol. Interface Eng. Ser. 48 (2005) 807–812.
[20] J. Horng, C. Wei, H. Tsai, A study of surface friction and particle friction between rough surfaces, Wear 267 (2009) 1257–1263.
[21] P. Sadowski, S. Stupkiewicz, Combined effect of friction and macroscopic deformation on asperity flattening, Tribol. Int. 43 (2010) 1735–1741.
[22] J. Jamari, D.J. Schipper, An elastic–plastic contact model of ellipsoid bodies, Tribol. Lett. 21 (2006) 262–271.
[23] M.A. Masen, M.B. de Rooij, D.J. Schipper, Micro-contact based modelling of abrasive wear, Wear 258 (2005) 339–348.
[24] M.B. de Rooij, G. van der Linde, D.J. Schipper, Modelling material transfer on a single asperity scale, Wear 307 (2013) 198–208.

[25] S. Shankar, M.M. Mayuram, A finite element based study on the elastic–plastic transition behaviour in a hemisphere in contact with a rigid flat, J. Tribol. 130 (2008) 1–6.
[26] K.L. Johnson, The correlation of indentation experiments, J. Mech. Phys. Solids 18 (1970) 115–126.
[27] J. Halling, R.D. Arnell, K.A. Nuri, The elastic–plastic contact of rough surfaces and its relevance in the study of wear, Proc. Inst. Mech. Eng., Part C: J. Mech. Eng. Sci. 202 (1988) 269–274.
[28] J. Halling, K. Nuri, Elastic–plastic contact of rough surfaces considering ellipsoidal asperities of work hardening multi-phase materials, Tribol Int. 24 (1991) 311–319.
[29] Y. Zhao, D.M. Maietta, L. Chang, An asperity micro-contact model incorporating the transition from elastic deformation to filly plastic flow, J. Tribol. 122 (2000) 86–93.
[30] H. Moes, Lubrication and Beyond, University of Twente, The Netherlands, 2000 ⟨http:/www.utwente.nl/ctw/tr/organisation/links/moes.pdf⟩ (University of Twente Lecture notes code 115531).
[31] L.P. Lin, J.F. Lin, An elasto plastic microasperity contact model for metallic materials, J. Tribol. 127 (2005) 666–672.
[32] E.J. Abbott, F.A. Firestone, Specifying surface quality—a method based on accurate measurement and comparison, Mech. Eng. 55 (1933) 569–572.
[33] R.L. Jackson, I. Green, A finite element study of elasto-plastic hemispherical contact against a rigid flat, J. Tribol. 127 (2005) 343–354.
[34] J.M. Challen, P.L.B Oxley, An explanation of the different regimes of friction and wear using asperity deformation mode, Wear 53 (1979) 229–243.
[35] W.C. Oliver, G.M. Pharr, Measurement of hardness and elastic modulus by instrumented indentation: advances in understanding and refinements to methodology, J. Mater. Res. 19 (2003) 3–20.
[36] W.C. Oliver, G.M. Pharr, An improved technique for determining hardness and elastic modulus using load and displacement sensing indentation experiments, J. Mater. Res. 7 (2003) 1564–1583.
[37] Y.Z. Hu, K. Tonder, Simulation of 3-D random rough surface by 2-D digital filter and fourier analysis, Int. J. Mach. Tools Manuf. 32 (1992) 83–90.
[38] A.A. Torrance, J. Galligan, G. Liraut, A model of the friction of a smooth hard surface sliding over a softer one, Wear 212 (1997) 213–230.
[39] E.M. Kopalinsky, A.J. Black, Metallic sliding friction under boundary lubricated conditions: investigation of the influence of lubricant at the start of sliding, Wear 190 (1995) 197–203.
[40] K. Hokkirigawa, K. Kato, An experimental and theoretical investigation of ploughing, cutting and wedge formation during abrasive wear, Tribol. Int. 21 (1988) 51–57.
[41] R.S. Timsit, C.V. Pelow, Shear strength and tribological properties of Stearic acid films (Part I) on glass and aluminium-coated glass, J. Tribol. 114 (1992) 150–158.